RSC Applied Interfaces

ROYAL SOCIETY OF CHEMISTRY

COMMUNICATION

View Article Online
View Journal | View Issue

Cite this: *RSC Appl. Interfaces*, 2024, **1**, 215

Received 6th September 2023,
Accepted 27th September 2023

DOI: 10.1039/d3lf00163f

rsc.li/RSCApplInter

A multifunctional organogel for constructing artificial light harvesting systems with excellent energy transfer efficiency†

Xinxian Ma, ‡* Jiahong Tang,‡ Tianqi Ren, Jiali Zhang, Yuehua Liang, Jiuzhi Wei and Enke Feng

Fluorescent gels with excellent physical properties were synthesised using polyvinyl alcohol (PVA)/telmisartan (Tmt) based on binary solvent. On this basis, artificial light-harvesting system with high energy-transfer efficiency and the antenna effect was constructed by adding the acceptors acridine yellow G and rhodamine B.

Nowadays, increasing attention is being paid to luminous energy as it is a 'green' and economical renewable energy source. Thus, an understanding of how to capture and use light energy is required. It was discovered that photosynthetic bacteria and green plants use photosynthesis for capturing, transferring and storing energy drawn from sunlight.[1,2] This motivated researchers to develop artificial light-harvesting systems (ALHSs) for efficient light collection,[3–11] and reports on ALHSs are increasing. Scientists have used energy-transfer efficiency (Φ_{ET}) and the antenna effect (AE) as parameters to evaluate the efficiency of ALHSs.[12–15] Cao *et al.* reported conjugated polymers that contained a column aromatic unit.[16] They used polymers as the primary material to bind a guest fluorescence molecule containing a triazole–alkyl–cyanide group and constructed an ALHS with an ultra-high AE. The AE can reach 35.9 and 90.4 in solutions and solid films, respectively. However, research has proven that high-efficiency ALHSs must fulfil three requirements: (1) the fluorescence spectrum of the donor should effectively overlap with the absorption band of the acceptor; (2) the donor must be sufficiently close to the recipient, with a distance of generally <10 nm; and (3) the spatial arrangement of the donor and recipient should be appropriate.[17,18] Efficient ALHSs typically utilise complex self-assembled structures,[19] such as nanocrystals, metal complexes, biohybrid complexes and dendritic polymers. These cases hinted that supramolecular gel systems can also help in the development of efficient gel ALHSs.[20,21]

However, research indicates supramolecular gels formed *via* non-covalent intermolecular interactions are easily destroyed by external shocks, which considerably limits the application of gels. Thus, how to build a mechanism for efficient ALHSs has become a complex problem. Moreover, hydrogels and organogels exhibit excellent ion transport[22,23] and adjustable mechanical properties owing to their unique three-dimensional mesh structure.[24] In addition, given the specificity of organogels, the desired properties, which include but are not limited to, self-repair,[25–27] antibacterial[28] and frost resistance,[29,30] can be achieved by adding functional units or modifying crosslinkers. Therefore, polymer organogels have been extensively researched as flexible new materials. In our previous research, we observed the excellent fluorescence properties of benzimidazole derivatives.[31]

Herein, we designed and synthesised a new polymer organogel with good fluorescence and physical properties. The carboxyl group and polyvinyl alcohol (PVA) can be cross-linked to form a stable polymer organogel in dimethyl sulfoxide (DMSO) through esterification at 120 °C. Then, we constructed efficient ALHSs with a high AE by adding the acceptors acridine yellow G (AYG) and rhodamine B (RhB), and confirmed the occurrence of energy transfer (Fig. 1).

The prediction that PVA and Tmt are cross-linked by esterification was demonstrated by ^{1}H nuclear magnetic resonance (^{1}HNMR) and Fourier transform infrared (FT-IR) (Fig. 2a). PVA's O–H proton signal was divided into three peaks: 4.302, 4.497 and 4.719 ppm (Fig. 2a(3)). However, in the PVA/Tmt organogel, the intensity of the signal peak of the O–H proton decreased evidently, and the O–H proton signals shifted from 4.497 to 4.539 ppm (Fig. 2a(1)), which proves that the hydroxyl groups in the PVA underwent a chemical reaction. In addition, the O–H proton signals of

College of Chemistry and Chemical Engineering, Ningxia Normal University, Guyuan 756000, P. R. China. E-mail: maxinxian@163.com

† Electronic supplementary information (ESI) available. See DOI: https://doi.org/10.1039/d3lf00163f

‡ These authors contributed equally to this work. They should thus be considered co-first authors.

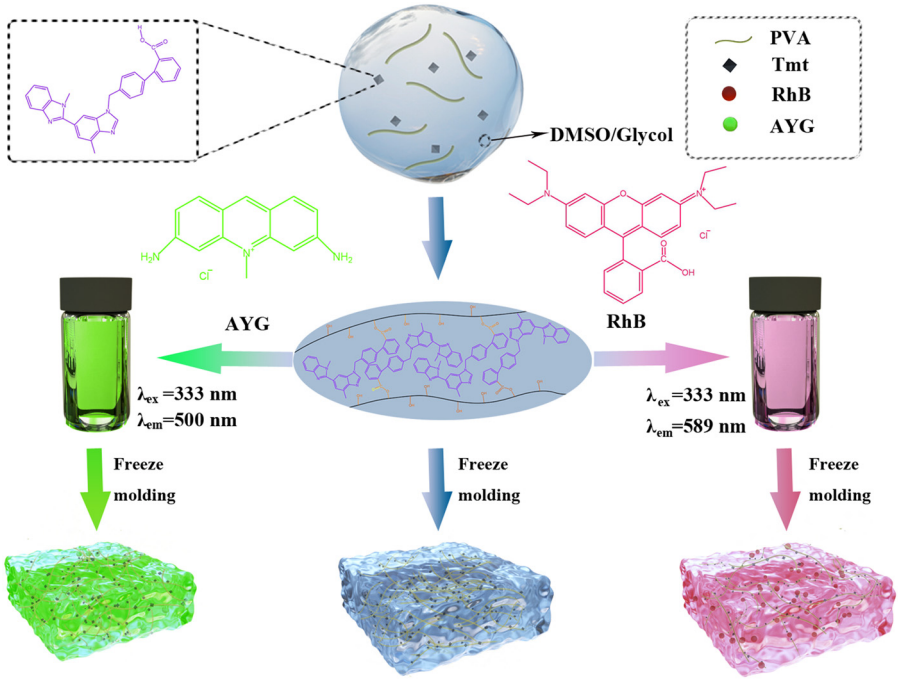

Fig. 1 Schematic of the formation, structure and intermolecular non-covalent interactions of the PVA/Tmt organogel and the prepared light-harvesting systems.

PVA shifted to a lower field at 4.539 ppm with the introduction of the electron-attracting group. In addition, some C–H proton signals of the PVA/Tmt organogel shifted by 0.058 ppm to a higher field (from 3.831 ppm to 3.773 ppm) as the oxygen atom formed a P–π conjugation with the carbonyl group. Then, electron delocalisation increased the C–H electron cloud density and decreased the chemical shift as the PVA hydroxyl connected to the carbonyl group. To further prove the conjecture that PVA and Tmt are cross-linked by esterification, we compared and analysed the Fourier transform IR spectroscopy (FT-IR) spectra of the solid PVA, the mixture of PVA and Tmt and the xerogel of the PVA/Tmt organogel (Fig. 2b). The typical peak of ν(C═O) in Tmt appeared at 1704.28 cm^{-1} (Fig. 2b(3)), and that of ν(C═O) in the PVA/Tmt organogel was at 1717.78 cm^{-1} (Fig. 2b(2)). Notably, the absorption band of ν(C═O) shifted towards a higher wavenumber at 1717.78 cm^{-1} after the introduction of an electron-withdrawing group. In addition, an absorption band of ν(C–O–C) was observed in the PVA/Tmt organogel at 1018.23 cm^{-1} (Fig. 2b(2)). The above analyses prove that the Tmt cross-linked with PVA through esterification.

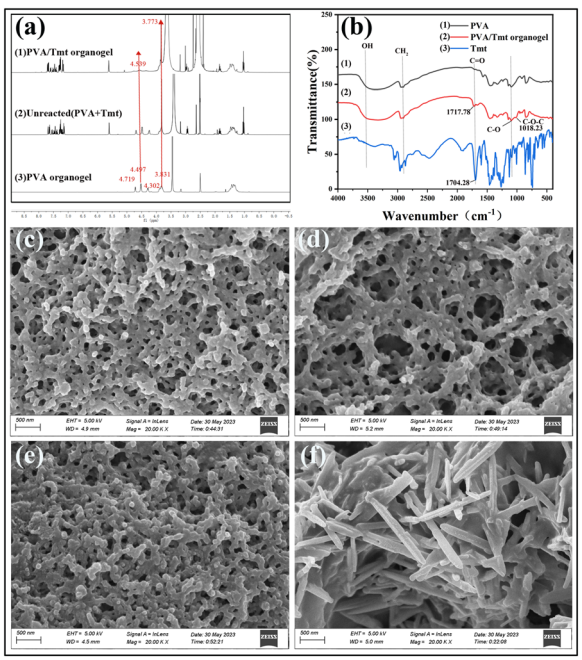

Fig. 2 (a) ^{1}H NMR and (b) FT-IR spectra of the different samples. Field-emission scanning electron microscopy (SEM) images of (c) PVA, (d) PVA/Tmt, (e) PVA/Tmt/RhB and (f) PVA/Tmt/AYG organogel samples.

We performed SEM to describe the morphological characteristics of the above samples (Fig. 2c–f). The xerogel of the PVA exhibited a layered morphology, which was observed *via* electron microscopy (Fig. 2c). Subsequently, given the esterification between PVA and Tmt, the morphology of the xerogel of the PVA/Tmt organogel exhibited an evident porous structure (Fig. 2d). Finally, after adding RhB and AYG to the mixture, the morphologies of the obtained xerogels became more densely porous and needle-like, respectively (Fig. 2e and f).

Subsequently, as can be observed in the charts shown in Fig. S1–S3,† the above three organogels had a considerably larger storage modulus (G') than loss modulus (G''). Moreover, the G' and G'' of the three above-mentioned

organogels were parallel to the frequency axis. Thus, the PVA/Tmt, PVA/Tmt/AYG and PVA/Tmt/RhB organogels all exhibited excellent gel properties in the above analysis.

After allowing them to settle for a while, the organogel samples were obtained. Then, the mechanical properties of the organogels were evaluated. As displayed in Fig. 3a, the PVA/Tmt organogel can be customised into various shapes (numbers and letters) through moulds, and showed a bluish violet fluorescence under a UV lamp. In addition, the fluorescence intensity and colour of the PVA/Tmt organogel system evidently changed in different ways with the addition of AYG and RhB dyes. Illuminated with 365 nm UV lamps, the PVA/Tmt/AYG organogel glowed with yellowish green hues and the PVA/Tmt/RhB organogel glowed with bright pink hues. The organogels also presented outstanding puncture resistance in a series of physical and mechanical tests (Fig. 3d). Similarly, the organogels can withstand a wide range of mechanical deformations without visible cracks or any breakage (Fig. 3b). Further, these organogels achieved high elongation at break and tensile strength in the stretching experiment (Fig. 3f and g). The PVA/Tmt/RhB organogel can quickly achieve a stretching strain of more than 800% without visible cracks or any breakage (Fig. 3f). In comparison, the PVA/Tmt/AYG organogel stretched to 830% strain (Fig. 3g). Fig. 3e exhibits the deformation of the PVA/Tmt organogel during compression. The organogels remained intact, and no liquid overflowed from them under heavy compression, proving that organogels have remarkable water-retaining capability and pressure resistance. Additionally, the compression test experiment proved their excellent pressure resistance (Fig. 3h). As presented in Fig. 3h, the pressure loads of the PVA/Tmt/RhB and PVA/Tmt/AYG organogels were 2.23 and 1.26 MPa, respectively. In addition, the organogels can successfully lift 2.1 kg without breaking in the load experiments (Fig. 3c).

The 'Tmt' type sample was turned into the 'PVA' type sample by sequentially cutting, heating at 90 °C and freezing. Using the same steps, the 'PVA' type sample can be turned into the 'Tmt' type sample (Fig. S4†). Moreover, the transmittances of the PVA/Tmt and PVA organogels in the visible range (350–800 nm) were tested using a UV spectrophotometer (Fig. S5†). The addition and reaction of Tmt molecules resulted in no substantial effect on the light transmittance of pure PVA organogels and enhanced that of other organogels. This finding is notably beneficial for visual abrasion applications.

To test the fluorescence properties of the obtained organogels, we cut them into sheets and used the patches to perform the fluorescence test. Fluorescence spectrometry revealed that the absorption band of the fluorescence dye AYG considerably overlapped with the emission band of the PVA/Tmt organogel (Fig. 4a). Therefore, the PVA/Tmt organogel was selected as a donor and AYG as the acceptor for the preparation of our ALHS. As displayed in Fig. 4b, the fluorescence intensity of the PVA/Tmt organogel gradually reduced at λ = 376 nm with the dropwise addition of AYG.

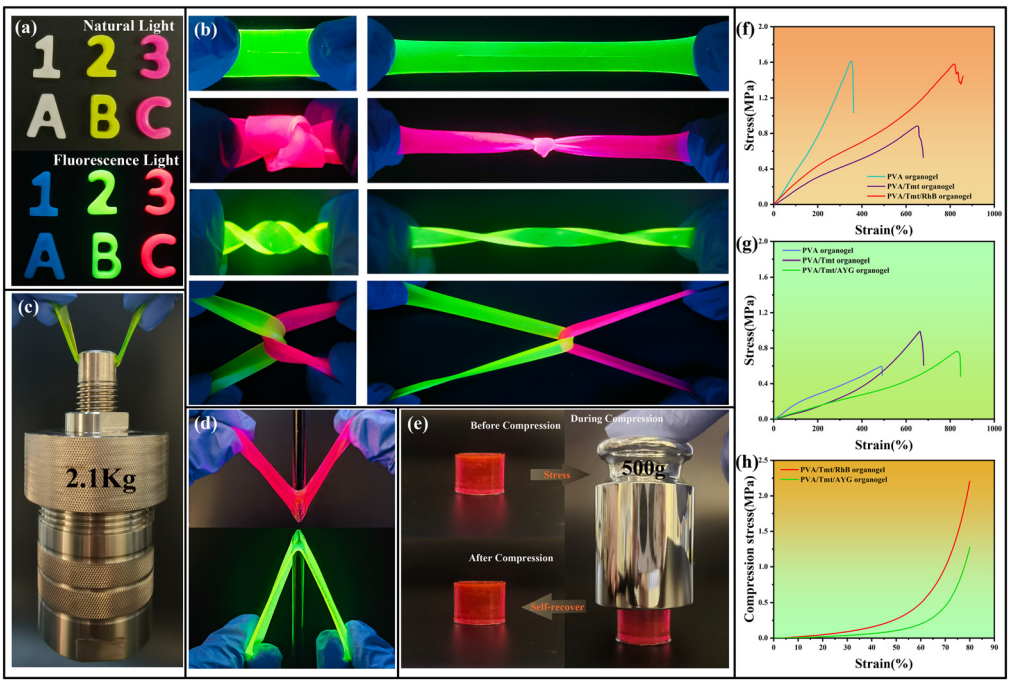

Fig. 3 (a) Photos of the organogels in different shapes under natural light and ultraviolet (UV) radiation. (b) Organogels can withstand a wide range of mechanical deformations. (c) PVA/Tmt/AYG organogels exhibited good load-bearing properties. (d) PVA/Tmt/RhB and PVA/Tmt/AYG organogels exhibited excellent puncture resistance. (e) Compression properties of the PVA/Tmt/RhB organogel. (f) Tensile stress–strain curve comparisons of the RhB organogel. (g) Tensile stress–strain curve comparisons of the AYG organogel. (h) Compression stress–strain curves of two organogels.

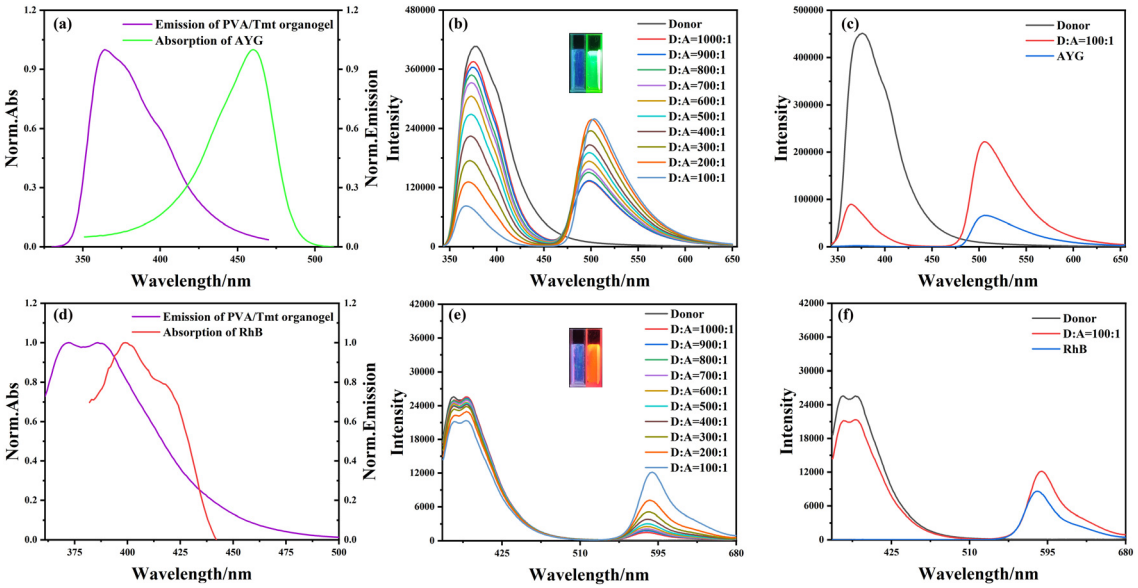

Fig. 4 (a) Normalised emission spectrum of PVA/Tmt organogel (λ_{ex} = 333 nm) and the absorption spectrum of AYG ([AYG] = 1×10^{-5} mol L^{-1}). (b) Fluorescence spectra of PVA/Tmt/AYG in the mixed solution with different concentrations of AYG. Inset: photographs of PVA/Tmt and PVA/Tmt/AYG organogel films ([Tmt] : [AYG] = 200 : 1). (c) Fluorescence-contrast spectra of PVA/Tmt/AYG organogel and pure AYG, with total AYG content the same in both ([Tmt] : [AYG] = 100 : 1). (d) Normalised emission spectrum of PVA/Tmt organogel (λ_{ex} = 350 nm) and the absorption spectrum of RhB ([RhB] = 1×10^{-5} mol L^{-1}). (e) Fluorescence spectra of PVA/Tmt/RhB in mixed solutions with different concentrations of RhB. Inset: photographs of PVA/Tmt and PVA/Tmt/RhB organogel films ([Tmt] : [RhB] = 200 : 1). (f) Fluorescence-contrast spectra of PVA/Tmt/RhB organogel and pure RhB, with total RhB content the same in both ([PVA/Tmt/RhB organogel] : [RhB] = 100 : 1).

Moreover, at an excitation wavelength of 333 nm, a new emission band appeared at λ = 500 nm. With the slow addition of AYG, the fluorescence intensity of the new emission band at λ = 500 nm gradually increased and reached a maximum at the following molar ratio: n_{donor} : $n_{acceptor}$ = 100 : 1. Thus, we hypothesised that energy transfer occurred in the PVA/Tmt/AYG organogel. Subsequently, we designed additional experiments to prove our speculation. We measured the fluorescence intensity of the pure acceptor (AYG) at a molar ratio of 100 : 1; at $n_{donor} : n_{acceptor}$ = 100 : 1 molar ratio, the fluorescence intensity at λ = 500 nm was notably higher than that of the pure acceptor (AYG), where both samples had the same total content of AYG, which proves the occurrence of energy transfer (Fig. 4c). Subsequently, the fluorescence lifetimes of the obtained samples were measured using a steady-state/lifetime spectrofluorometer. The fluorescence lifetimes of the PVA/Tmt organogel and PVA/Tmt/AYG organogel were fitted as a double exponential decay. The fluorescence lifetimes of the PVA/Tmt organogel are τ_1 = 0.93 ns, τ_2 = 4.30 ns, and τ = 2.74 ns. The fluorescence lifetimes of the PVA/Tmt/AYG organogel are reduced to τ_1 = 0.91 ns, τ_2 = 1.85 ns, and τ = 1.21 ns, which suggests that energy from the donor is transferred to the acceptor (Fig. S6 and S7, Table S1†). Further, the fluorescence quantum yield (QY) of the obtained samples was measured. As shown in Fig. S8,† the fluorescence QY of the PVA/Tmt/AYG organogel was measured to be 43.10% at the selected wavelength range 450–700 nm. All the above analyses confirmed the successful construction of the PVA/Tmt/AYG ALHS.

Similarly, we constructed an additional ALHS using RhB as the fluorescence acceptor given the substantial overlap between the absorption band of the fluorescence dye RhB and the emission band of the PVA/Tmt organogel (Fig. 4d). Fig. 4e shows that the fluorescence intensity of the PVA/Tmt organogel gradually decreased at λ = 387 nm with the dropwise addition of RhB. Furthermore, at an excitation wavelength of 350 nm, a new emission band appeared at λ = 589 nm. With the slow addition of RhB, the fluorescence intensity of the new emission band at λ = 589 nm gradually increased and reached a maximum at the molar ratio of $n_{donor} : n_{acceptor}$ = 100 : 1. Based on the above phenomena, we designed additional experiments to prove that energy transfer occurred in the PVA/Tmt/RhB organogel. The fluorescence intensity of the pure acceptor (RhB) in the system at a molar ratio of 100 : 1 was measured (the quantity of RhB was not changed). Similar to the PVA/Tmt/AYG organogel, when the molar ratio was $n_{donor} : n_{acceptor}$ = 100 : 1, the fluorescence intensity at λ = 589 nm was notably higher than that of the pure acceptor (RhB) (both had the same total content of RhB) in the comparison of the obtained fluorescence spectra ($n_{donor}/n_{acceptor}$ = 100 : 1; pure RhB), evidencing the occurrence of the energy transfer process (Fig. 4f). Subsequently, the fluorescence lifetimes of the obtained samples were measured using the steady-state/lifetime spectrofluorometer. The results show that the decay curves of the obtained PVA/Tmt and PVA/Tmt/RhB organogels were fitted with a double exponential model. The fluorescence lifetimes of the PVA/Tmt organogel are τ_1 = 0.7645 ns, τ_2 = 2.73 ns, and τ = 1.27 ns. The fluorescence lifetimes of the

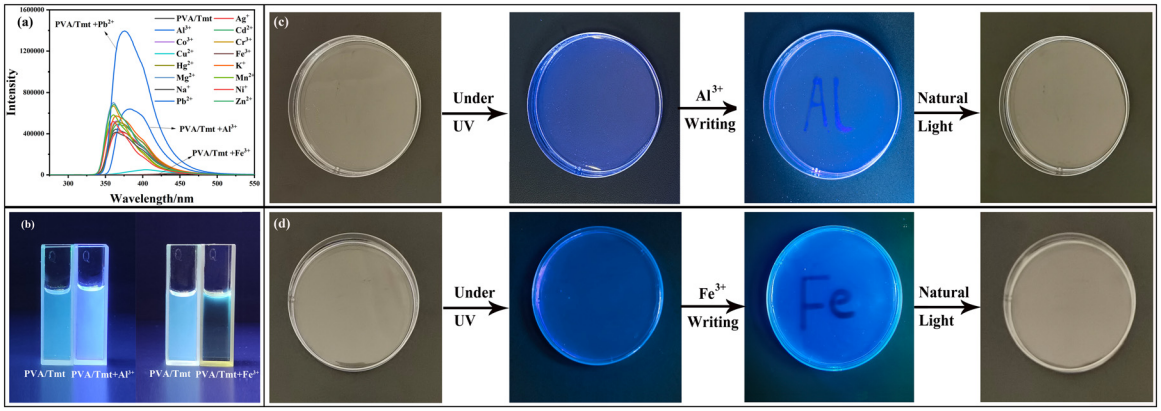

Fig. 5 (a) Fluorescence spectra of the PVA/Tmt organogel in the presence of equiv. metal ions (Cr^{3+}, Zn^{2+},Co^{3+}, K^{+}, Al^{3+}, Mn^{2+}, Hg^{2+}, Fe^{3+}, Mg^{2+}, Cu^{2+}, Cd^{2+}, Pb^{2+}, Ni^{2+}, Ag^{+} and Na^{+}, 0.1 mol L^{-1}) (λ_{ex} = 333 nm). (b) Photos of the PVA/Tmt, PVA/Tmt–Al^{3+} ([Al^{3+}] = 5 × 10^{-6} mol), PVA/Tmt and PVA/Tmt–Fe^{3+} ([Fe^{3+}] = 5 × 10^{-6} mol) under UV lamp irradiation. (c) The message written on the PVA/Tmt organogel using the Al^{3+} solution under natural light and UV lamps. (d) The message written on the PVA/Tmt organogel using the Fe^{3+} solution under natural light and UV lamps.

PVA/Tmt/AYG organogel are reduced to τ_1 = 0.7642 ns, τ_2 = 2.45 ns and τ = 1.18 ns, which suggests that energy from the donor is transferred to the acceptor (Fig. S9 and S10, Table S2†). The fluorescence QY of the obtained samples was measured in a similar manner. The fluorescence QY of the PVA/Tmt/RhB organogel reached 51.06% at the selected wavelength range of 520–700 nm (Fig. S11†). All the above analyses confirmed the successful construction of a PVA/Tmt/RhB ALHS.

To evaluate the efficiency of the PVA/Tmt/AYG and PVA/Tmt/RhB ALHSs, the energy-transfer efficiency (Φ_{ET}) and AE were used as parameters. The Φ_{ET} values of the PVA/Tmt/AYG ALHS were 8.60%, 11.45%, 16.40%, 20.13%, 27.07%, 35.97%, 46.80%, 59.20%, 70.20% and 82.77% when the donor-to-acceptor molar ratios were 1000 : 1, 900 : 1, 800 : 1, 700 : 1, 600 : 1, 500 : 1, 400 : 1, 300 : 1, 200 : 1 and 100 : 1, respectively (Fig. S12†). Similarly, the Φ_{ET} values for the PVA/Tmt/RhB ALHS were calculated to be 0.13%, 0.96%, 1.42%, 2.48%, 3.87%, 4.51%, 5.28%, 6.67%, 10.18% and 16.58%, when the molar ratios of the donor-to-acceptor were 1000 : 1, 900 : 1, 800 : 1, 700 : 1, 600 : 1, 500 : 1, 400 : 1, 300 : 1, 200 : 1 and 100 : 1, respectively (Fig. S13†). Thus, the Φ_{ET} values substantially increased with the dropwise addition of AYG into the PVA/Tmt organogel system and reached a staggering peak of 82.77% when the molar ratio of donor-to-acceptor was 100 : 1 (Fig. S14(a)†). With the dropwise addition of RhB to the PVA/Tmt organogel system, the Φ_{ET} values increased remarkably as well, with a final peak of 16.58% attained when the molar ratio of the donor-to-acceptor was 100 : 1 (Fig. S14(b)†). In addition, analysis of the normalised intensity revealed that the AE of the PVA/Tmt/AYG and PVA/Tmt/RhB ALHSs were 16.8690 and 1.7889, respectively, indicating that the PVA/Tmt/AYG ALHS had an excellent AE (Fig. S15 and S16†). These results demonstrate the great efficiency and economy of the PVA/Tmt/AYG ALHS. Overall, from the above analyses, the PVA/Tmt/AYG and PVA/Tmt/RhB ALHSs exhibited good light-capturing effect.

The effects of metal ions on the fluorescence properties of the PVA/Tmt organogels were tested using nitrate solutions with the same concentration of Na^{+}, Ni^{2+}, Pb^{2+}, Zn^{2+}, Cd^{2+}, Hg^{+}, Cu^{2+}, Fe^{3+}, Co^{2+}, Al^{3+}, Cr^{3+}, K^{+}, Mg^{2+}, Ag^{+} or Mn^{2+}. With the addition of Al^{3+}, the fluorescence spectrum of the PVA/Tmt organogel redshifted (Fig. 5a), accompanied with the colour emission changing from bluish purple to green under 333 nm UV light (Fig. 5b). In addition, the fluorescence intensity of the PVA/Tmt organogel doubled with the addition of Pb^{2+} (Fig. 5a). Moreover, the PVA/Tmt organogel was quenched after the addition of Fe^{3+} (Fig. 5a and b), due to the paramagnetism causing fluorescence quenching of the PVA/Tmt organogel by Fe^{3+}.[32,33] Prompted by this finding, we attempted to write on the top of the PVA/Tmt organogel using an aqueous solution containing Al^{3+} and Fe^{3+}, due to the toxicity of Pb^{2+}. Notably, the fluorescence changed from bluish violet to dark blue under a 333 nm UV light when the aqueous solution containing Al^{3+} was used to write on the PVA/Tmt organogel, which means that the 'Al^{3+}' writing can be observed (Fig. 5c). However, no such phenomenon can be observed under natural light instead of UV light, suggesting that the 'Al^{3+}' writing cannot be retained under natural light. In addition, fluorescence quenching could be clearly observed when the aqueous solution containing Fe^{3+} was used to mark the PVA/Tmt organogel, no such phenomenon could be observed when natural light was used instead of UV light (Fig. 5d). Based on the above findings, 'Al^{3+}' and 'Fe^{3+}' can be written on the PVA/Tmt organogel, which is only visible under the 333 nm UV light. Thus, the PVA/Tmt organogel can be used as a writing and information anticounterfeiting material.

Conclusions

Fluorescent gels with unique mechanical and physical properties were synthesised using two ratios of PVA/Tmt based on DMSO–ethylene glycol binary solvent. The prepared

gels exhibited many excellent physical properties, such as tensile property, compression performance, transmittance and lifting performance. In addition, two different ALHSs were successfully constructed through Forster resonance energy transfer, which occurred from the donor (PVA/Tmt organogel) to the acceptor (AYG or RhB), with the addition of a fluorescent dye (AYG or RhB) to the PVA/Tmt organogel. Notably, the Φ_{ET} values of the two ALHSs were 82.77% (PVA/Tmt/AYG organogel) and 16.58% (PVA/Tmt/RhB organogel) when the molar ratio was $n_{donor}:n_{acceptor}$ = 100:1. In addition, the AE values of the two ALHSs were 16.8690 (PVA/Tmt/AYG organogel) and 1.7889 (PVA/Tmt/RhB organogel), indicating that the PVA/Tmt/AYG ALHS had an excellent AE. Furthermore, the PVA/Tmt organogel could be used as a writing and an anticounterfeiting material. This research provides a new idea and basis for the construction of ALHSs based on multiperformance fluorescent organogels prepared using cross-linking agents such as PVA.

Author contributions

Xinxian Ma: conceptualization, resources, funding acquisition, writing – review & editing. Jiahong Tang: methodology, investigation, writing – original draft. Tianqi Ren and Jiali Zhang: materials characterization, performance tests. Jiuzhi Wei, Yuehua Liang and Enke Feng: performance tests.

Conflicts of interest

There are no conflicts to declare.

Acknowledgements

This work was supported by the National Natural Science Foundation of China (No. 21961029), the Natural Science Foundation of Ningxia, China (No. 2020AAC02031), the Science and Technology Foundation of Guyuan, China (No.: 2021GYKYF003), which are gratefully acknowledged.

Notes and references

1 Y. Hu, P. Jia, C. Zhang, X. Xu, Y. Niu, X. Zhao, Q. Xu, L. Xu and H. Yang, *Org. Chem. Front.*, 2021, **8**, 5250–5257.
2 S. Yan, Z. Gao, H. Yan, F. Niu and Z. Zhang, *J. Mater. Chem. C*, 2020, **8**, 14587–14594.
3 G. Sun, W. Qian, J. Jiao, T. Han, Y. Shi, X. Hu and L. Wang, *J. Mater. Chem. A*, 2020, **8**, 9590–9596.
4 H. Qian, T. Xiao, R. Elmes and L. Wang, *Chin. Chem. Lett.*, 2023, **34**, 108185.
5 K. Diao, D. Whitaker, Z. Huang, H. Qian, D. Ren, L. Zhang, Z. Li, X. Sun, T. Xiao and L. Wang, *Chem. Commun.*, 2022, **58**, 2343–2346.
6 P. Chen, Y. Weng, L. Niu, Y. Chen, L. Wu, C. Tung and Q. Yang, *Angew. Chem., Int. Ed.*, 2016, **55**, 2759–2763.
7 H. Peng, Y. Chen, Y. Zhao, Q. Yang, L. Wu, C. Tung, L. Zhang and Q. Tong, *Angew. Chem., Int. Ed.*, 2012, **51**, 2088–2092.
8 X. Ma, J. Yue, B. Qiao, Y. Wang, Y. Gao, T. Ren, J. Tang, E. Feng, Z. Li and X. Han, *Polym. Chem.*, 2022, **13**, 3270–3274.
9 T. Xiao, W. Zhong, L. Zhou, L. Xu, X. Sun, R. Elmes, X. Hu and L. Wang, *Chin. Chem. Lett.*, 2019, **30**, 31–36.
10 V. Singh, B. Dwivedi, Y. Kumar and D. Pandey, *New J. Chem.*, 2021, **45**, 1677–1685.
11 J. Ji, S. Chereddy, Y. Ren, X. Chen, D. Su, Z. Zhong, T. Mori, Y. Inoue, W. Wu and C. Yang, *J. Photochem. Photobiol., A*, 2018, **355**, 78–83.
12 T. Xiao, H. Xiao, Y. Shen, C. Wei, D. Ren, L. Zhang, Z. Li, L. Wang and X. Sun, *Mater. Today Chem.*, 2022, **24**, 100833.
13 T. Xiao, X. Wei, H. Wu, K. Diao, Z. Li and X. Sun, *Dyes Pigm.*, 2021, **188**, 109161.
14 S. Guo, Y. Song, Y. He, X. Hu and L. Wang, *Angew. Chem., Int. Ed.*, 2018, **57**, 3163–3167.
15 M. Hao, G. Sun, M. Zuo, Z. Xu, Y. Chen, X. Hu and L. Wang, *Angew. Chem., Int. Ed.*, 2020, **59**, 10095–10100.
16 L. Xu, Z. Wang, R. Wang, L. Wang, X. He, H. Jiang, H. Tang, D. Cao and B. Tang, *Angew. Chem., Int. Ed.*, 2020, **59**, 9908–9913.
17 H. Peng, L. Niu, Y. Chen, L. Wu, C. Tung and Q. Yang, *Chem. Rev.*, 2015, **115**, 7502–7542.
18 C. Curutchet and B. Mennucci, *Chem. Rev.*, 2017, **117**, 294–343.
19 L. Ji, Y. Sang, G. Ouyang, D. Yang, P. Duan, Y. Jiang and M. Liu, *Angew. Chem., Int. Ed.*, 2019, **58**, 844–848.
20 Y. Wang, Y. Gao, J. Tang, T. Ren, J. Zhang, Y. Liang, J. Wei, E. Feng and X. Ma, *ACS Appl. Polym. Mater.*, 2023, **5**, 3809–3816.
21 X. Wang, W. Zhou, R. Xu, Y. Xu, H. Song, H. Li and J. Wang, *J. Colloid Interface Sci.*, 2023, **645**, 466–471.
22 X. Ma, Y. Geng, Y. Gao, J. Zhang, Y. Wang, Y. Lai, T. Ren and J. Tang, *Soft Matter*, 2022, **18**, 5166–5170.
23 M. Lee, S. An, B. Joshi, S. Latthe and S. Yoon, *ACS Appl. Mater. Interfaces*, 2013, **5**, 1232–1239.
24 X. Liu, Q. Zhang, L. Duan and G. Gao, *ACS Appl. Mater. Interfaces*, 2019, **11**, 6644–6651.
25 X. Ma, Y. Gao, Y. Geng, J. Zhang, Y. Lai, Y. Wang, J. Tang and T. Ren, *ACS Appl. Energy Mater.*, 2022, **5**, 9303–9308.
26 E. Feng, W. Gao, J. Li, Q. Yang, Z. Li, X. Ma, T. Zhang and Z. Yang, *ACS Sustainable Chem. Eng.*, 2020, **8**, 3311–3320.
27 J. Zhao, J. Gong, G. Wang, K. Zhu, K. Ye, J. Yan and D. Cao, *Chem. Eng. J.*, 2020, **401**, 125456.
28 Y. Ma, J. Yao, Q. Liu, T. Han, J. Zhao, X. Ma, Y. Tong, G. Jin, K. Qu and B. Li, *Adv. Funct. Mater.*, 2020, **30**, 2001820.
29 X. Ma, Y. Gao, Y. Geng, J. Zhang, Y. Lai, Y. Wang, T. Ren, J. Tang and E. Feng, *ACS Appl. Energy Mater.*, 2023, **6**, 1501–1510.

30 E. Feng, X. Li, J. Li, Z. Yan, G. Zheng, W. Gao, Z. Li, X. Ma and Z. Yang, *J. Mater. Chem. C*, 2021, **9**, 15530.
31 X. Zhu, Q. Lin, Y. Zhang and T. Wei, *Sens. Actuators, B*, 2015, **219**, 38–42.
32 X. Tang, Y. Wang, J. Han, L. Ni, L. Wang, L. Li, H. Zhang, C. Li, J. Li and H. Li, *Spectrochim. Acta, Part A*, 2018, **191**, 172–179.
33 Z. Zhang, F. Li, C. He, H. Ma, Y. Feng, Y. Zhang and M. Zhang, *Sens. Actuators, B*, 2018, **255**, 1878–1883.